University of Thi_Qar Journal for Engineering Sciences
http://www.doi.org/10.31663/tqujes.11.2.396(2021)
Vol 11.2(April 2021)

ISSN :2664- 5572 (online)
ISSN:2664-5564 (print)
Available at http://jeng.utq.edu.iq
utjeng@ utq.edu.iq

Numerical study for the effect of diameter and height for inline micro jets arrays arrangement

Asst. Lec. Ghassan A. Abd[‡], Dr. Ahmed A. Ouda[†], and Afnan F. Jabber[†]
[‡] Mechanical Engineering Department, University of Thi-Qar, Iraq, Ghassanadnan37@gmail.com.
[†] Mechanical Engineering Department, University of Thi-Qar, Iraq, ouda1978@utq.edu.iq.
[†] Mechanical Engineering Department, University of Thi-Qar, Iraq, fannonfaz@gmail.com

Abstract

In this research a numerical simulation of the micro-jet system used to cool an electronic chip was performed, as it was of type multijet, the basic idea of how the impingement cooling method works on the micro jet cooling array was provided by these simulations that consisted of a variety of parameters: Reynolds number (500-3000), diameter of jets (150-750) µm, number of jets (11,13,15,19,21), and distance between jets and target (450,337.5,225,168.75,112.5) µm. Shear stress transport (SST) K-ω model was used because it's able to predict the laminar to turbulent transition according to previous research. The input heat flux =36421 w/m² and area of plat (28700×28700) µm². The result shows the performance was improved when the jet diameter was increased, as the highest value of the Nu was obtained at (d = 600µm) and the losses were reduced. Also, the performance improved when the number of jets was increased.

Keywords: micro jet, electronics cooling, micro turbulent, jet array.

Nomenclature

Re	Reynolds number (U_oD/v for a jet)
Nu	Nusselt number $Nu = hD_h/K_c$
h	Convective heat transfer coefficient
U or u	Fluid velocity component
u_i	General velocity vector
U_o	Jet initial speed, average
v	Fluid velocity
β	Turbulence model constant
D	Nozzle diameter
K_c	Fluid thermal conductivity
Pr	Prandtl number = fluid thermal diffusivity/fluid viscosity
µ	Fluid viscosity
ρ	Fluid density
σ	Standard deviation function (normalized)
ω	Fluctuation frequency (used in k–ω model)
T	Temperature
ε	Turbulent kinetic energy dissipation rate
σ_{ij}	Steady stress tensor
τ_{ij}	Turbulent stress tensor (Reynolds stress tensor)
α	Turbulence model constant
x	Axial coordinate
y	Vertical coordinate
z	Horizontal coordinate
L	Distance between jets and the hot piece

1. Introduction

In recent years, electronic equipment cooling technology has been a critical prerequisite due to the continuous minimization of electronic components despite rising heat fluxes within this equipment by several orders of magnitudes **[1]**. Heat fluxes seen in processors and power electronics are quickly approaching a level that cannot be easily accommodated by forced air convection over finned heat sinks. Therefore, it is necessary to use a cooling method that is available to meet heat rejection needs **[2]**.

The microscale jet impingement system is known to produce high heat transfer rates as compared to other single heat transfer techniques. For this reason, jet

impingement has many industrial applications. In addition to thermal control application such as de-icing of aircraft wings and engine nacelles **[3]**, this technique is also used in conventional –scale applications such as cooling of gas turbine airfoils and electronic chips, drying of paper and textile, or other thin layers of films, annealing of metals, and glass tempering operations **[4]**.

Micro jet also uses in Light-Emitting Diodes (LEDs) in contemporary years because of their advantages compared with prevalent light sources. Theoretically, it has many special advantages such as high efficiency, good reliability, long life, variable color, and low-power consumption **[5]**. The flowing shape of an impinging jet divided into three regions: (a) A free jet region. (b) the stagnation region or deceleration region. (c) wall jet region **[6]**.

Many researchers have studied the shape of an impinging jet flow and the effect of turbulence such as Xiaoping et al **[7]** it was found that the higher micro pump flow rate would result in improved cooling efficiency, but it also increases the cost of operation, Browne et al **[8]** it was found that The chamber pressure of the 54 μm array differed by less than 5 kpa, this is due to the higher performance of the impingement region. , Husain et al **[9]** The results proved the increased stagnation heat transfer coefficient was caused by the increased jet Reynolds number, which subsequently increased jet impingement h_{av}. Rattner **[10]** The results proved the heat transfer coefficient increases as the Reynolds number increases. Robinson et al **[11]** results found that with the initial rise in flow rate, the total thermal conductance increases rapidly and the rate of increase in the pressure drop and related pumping power increases with the rising flow rate. Zahoor et al **[12]** the results showed a significant cooling of the gas in the Chamber. Wei et al **[13]** it was found that the k-ω model and SST transition model show good compliance with the temperature of the measured chip. Shin et al **[14]** the study showed The wall jet flow in the transverse direction approaches the channel side walls, creating vortices, which impede jets' deflection

2.Governing equations:

Modeling of the turbulent flow, incompressible except for the cases where the Mach number is high, is based on using the well-established mass, momentum, and energy conservation equations based on the velocity, pressure, and temperature:

$$\frac{\partial \overline{u_i}}{\partial x_i} = 0 \qquad (1)$$

$$\rho \frac{\partial u_i}{\partial t} + \rho \overline{u_\iota} \frac{\partial \overline{u_J}}{\partial x_j} = -\frac{\partial \bar{p}}{\partial x_i} + \frac{\partial \sigma_{ij}}{\partial x_j} + \frac{\partial \tau_{ij}}{\partial x_j} \qquad (2)$$

$$\rho \overline{u_\iota} = -\frac{\partial \bar{p}}{\partial x_i} + \frac{\partial}{\partial x_i}\left[\mu\left(\frac{\partial \overline{u_\iota}}{\partial x_j} + \frac{\partial \overline{u_j}}{\partial x_i}\right)\right] + \frac{\partial}{\partial x_i}(-\rho \overline{u_\iota}\overline{u_j}) \qquad (3)$$

$$\rho c_p \overline{u_J} \frac{\partial \bar{T}}{\partial x_j} = \sigma_{ij} \frac{\partial \overline{u_\iota}}{\partial x_i} + \frac{\partial}{\partial x_i}\left(\frac{\mu c_p}{Pr} \frac{\partial \bar{T}}{\partial x_i}\right) + \frac{\partial}{\partial x_j}\left(-\rho c_p \overline{\acute{u_J}\acute{T}}\right) + \overline{\mu(\frac{\partial \acute{u_\iota}}{\partial x_J} + \frac{\partial \acute{u_J}}{\partial x_\iota})\frac{\partial \acute{u_\iota}}{\partial x_J}} \qquad (4)$$

$$\sigma_{ij} = \mu\left(\frac{\partial \overline{u_\iota}}{\partial x_j} + \frac{\partial \overline{u_J}}{\partial x_i}\right) \qquad (5)$$

$$\tau_{ij} = -\rho \overline{u_\iota \acute{u_J}} \qquad (6)$$

$$\rho U_j \frac{\partial k}{\partial x_j} = \tau_{ij} \frac{\partial U_i}{\partial x_j} - \beta^* \rho k \omega + \frac{\partial}{\partial x_j}\left[(\mu + \sigma^* \acute{\mu}) \frac{\partial k}{\partial x_j}\right] \qquad (7)$$

$$\rho U_j \frac{\partial \omega}{\partial x_j} = \alpha \frac{\omega}{k} \tau_{ij} \frac{\partial U_i}{\partial x_j} - \beta \rho \omega^2 + \frac{\partial}{\partial x_j}\left[(\mu + \sigma \acute{\mu}) \frac{\partial \omega}{\partial x_j}\right] \qquad (8)$$

$$\acute{\mu} = \frac{\rho \kappa}{\omega} \qquad (9)$$

$$\varepsilon = \beta^* \omega k \qquad (10)$$

3. Numerical Modeling:

The model studied contains different forms of microjet The model contains the hot piece, which is usually made of aluminum because aluminum has a density around one third that of steel or copper making it one of the lightest commercially available metals and ability to resist rust, the thermal conductivity of aluminum is about three times greater than that of steel and its little cost **[15]**. A major parameter for evaluating heat transfer coefficients is the Nusselt number,

$$Nu = hD_h/K_c \qquad (11)$$

where h is the convective heat transfer coefficient:

$$\text{Re} = U_o D/v \qquad (12)$$

$$Q = mc_{p,j}(T_{EX} - T_{In}). \qquad (13)$$

The graphic shown in Fig. (1) represents the model that was worked on. the dimensions of the piece are (28700×28700) μm the height of the jet (500) μm. In Fig. 2 simple drawing for clarification shows the areas of entry of air at the top through the jets and the areas of its exit from the sides. Also, there are some important dimensions such as the distance between the jets represents (X) which was derived through the dimensions of the piece and the number of the jets as in the equation below, except the first jet, which is a distance ($\frac{X}{2}$)from the edge of the piece. The dimension (L) represents distance from the upper wall to the hot piece. This distance is occupied by air, so there is no heat conduction. The governing equations and the boundary condition were numerically solved using computational fluid dynamic (CFD) to calculate the outlet temperature, hot part temperature, outward pressure, an inward pressure. The model used in this paper is several of micro jet which enters the air and the hot piece that is in contact with the slide.

$$x = \frac{2w}{n} \qquad (14)$$

3. 1. model design

This step is done using the ANSYS software. ANSYS is used to draw geometric dimensions. Drawing includes identifying the axes to draw on and design shapes. Shapes are grouped into one body and a choice is either fluid or solid. For our work a fluid is chosen because we want to know the distribution of temperatures and pressure when air flows.

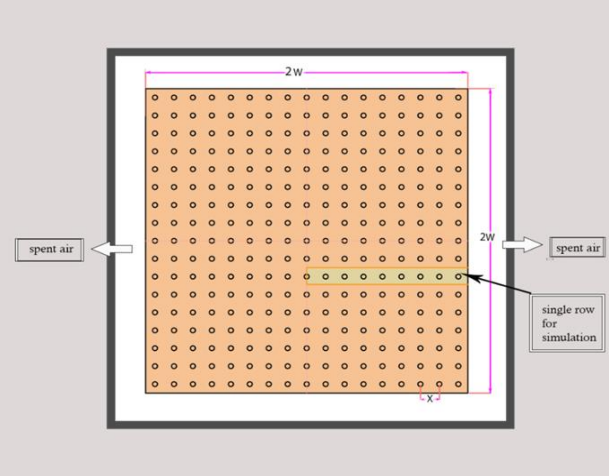

Fig. 1 Schematic of the jet impingement plate

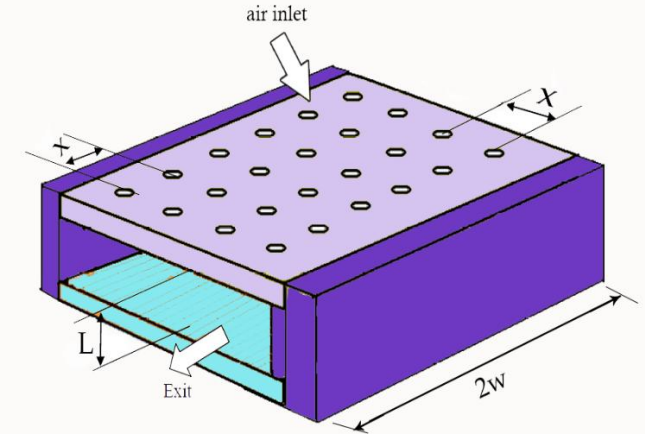

Fig.2 Schematic representation of non-dimensional geometric parameters **[16]**

3. 2. Mesh construction

This step was also done in ANSYS. starting by naming each surface in the body and then choosing the type of grid. There are several forms of grids and choose the form that provides the appropriate distribution and should be by the specifications of the computer. The figure below shows the grid shape chosen.

To obtain accurate results the network test was done and when obtaining close results, the network used was installed, and in the table (1) note attempts for several networks.

Table 1 Attempts to choose the grid

Mesh size	Outlet temperature (K)
Element=262826	314.9
Nodes=1301555	314.32
Nodes=1023590	314.33
Nodes=926905 Element=855266	314.38

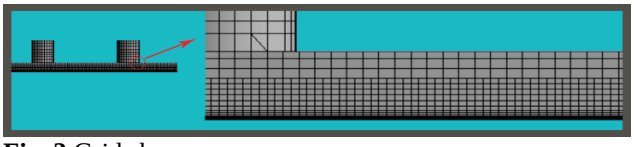

Fig. 3 Grid shape

3. 3. establish and apply boundary conditions

Where the boundary conditions are set for some of the parts that have been named, one of the important steps here is to choose the type of model viscosity, we select (Transition SST) **[16]**, **[17]**, which is considered one of the best types used in the micro jet according to previous research. Table (2) shows the boundary conditions.

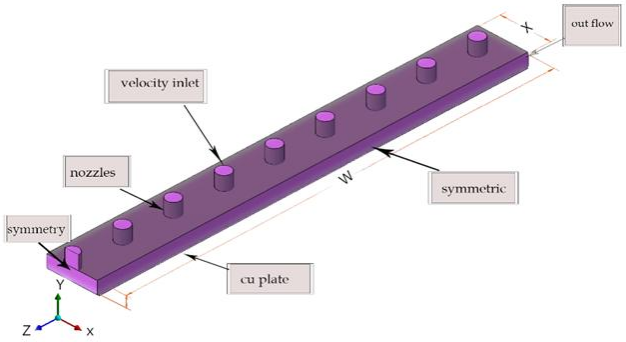

Fig. 4 Boundary conditions

Table (2) Applied boundary conditions

Location	Boundary conditions	Description
Jet inlet (x, y, z)	T=298 k V=v_{in}	Velocity inlet
Jet outlet (x, y ,z)		Out flow
Hot wall (x, y, z)	Q= 36421 w/m²	wall

4.Results and Discussions

4.1. Validation:

This model has been validated with the numerical model presented by the researchers mentioned in [13], data validation is vital to ensure the data is clean, correct, and useful so running validation on data means the ability to confident with the results. The numerical model given by researchers is a multiple jet impingement system that has a plate area (29×29) mm² square inline array consisting of jets with 400 µm diameter. The boundary conditions for this work are inlet temperature equal 298 k, heat flux about 14268 w, and velocity is variable with Reynolds number, which ranges from 400 to 2000. In figure (5) note the difference between the results obtained and the results of [13] and it appears from the figure that the results are compatible and that the largest percentage of error was 10.5%. This ratio is found by:

$$\frac{Nu_{for\ the\ current\ study} - Nu_{for\ the\ aforementioned\ study}}{Nu_{for\ the\ current\ study}} * 100\% \quad (15)$$

The results of five values were collected and divided by their number to find the total percentage.

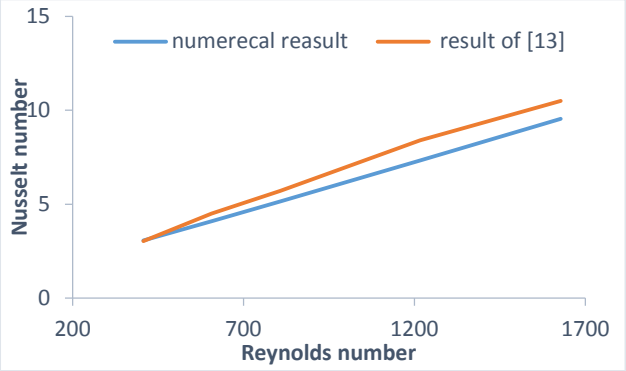

Fig. 5 A comparison between the results obtained and the research results [13]

4.2. Effect of the diameter change

Fig. 6.a shows the change in the value of Nu when changing the diameter of the jet in the circular jet for jets number (n=17) and height (L=450µm), as it was found that the value of Nu increases with the increase of the jet diameter because the increase in the diameter leads to an increase in the flow rate, which increases the thermal transfer rate (Q) and thus increases the thermal transfer coefficient (h) and increases the Nu.

Fig.6.b shows the relationship of the pressure drop with the change of the jet diameter in the circular jet, the pressure drop within this system is important because it reflects the mass flow rate and the energy consumption rate. Therefore, it is important to calculate the pressure drop inside the system. The reason for the pressure drop is the result of kinetic energy losses when leaving the nozzle and the pressure drop at the wall due to viscosity losses**,** two values of the flow rate were chosen (m=5.56E-5), (m=4.64E-5) and fixed each time so that the effect of the diameter increase on the pressure drop can be observed. note from the diagram that as the jet diameter increases, the pressure drop decreases because when the diameter decreases, the friction losses decrease and decrease cross-flow velocity, a decrease in the value of (Δp) means a decrease in the energy consumed.

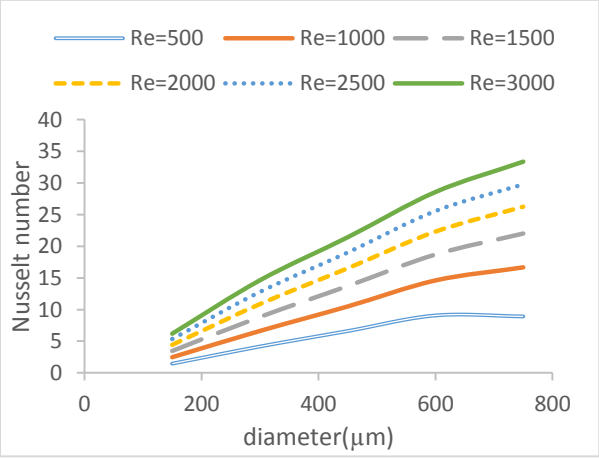

a

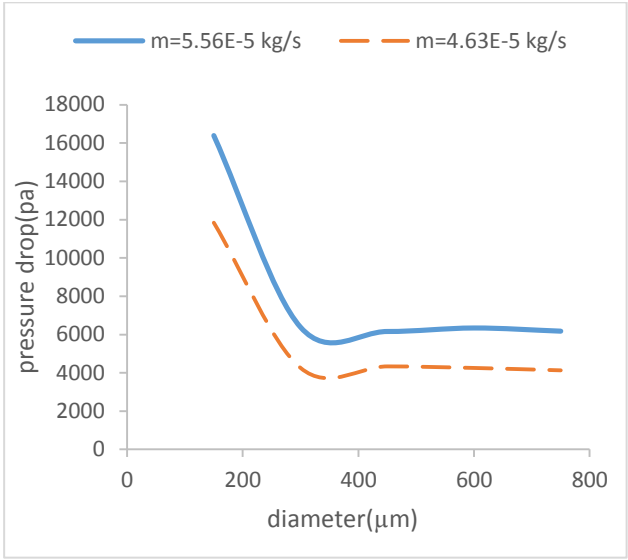

b

Fig. 6.a. Variation of Nusselt number (Nu) with diameter in circular jet for (n=17) and (L=450 µm), **b.** Variation of pressure drop (Δp) with diameter for Two values of flow rate in the circular jet for (n=17) and (L=450 µm)

4.3. Effect of changing distance between jets and the hot piece (height)

Fig.7.a represents the relationship between the distance between the jets and the hot piece (height) and Nu value in the circular jet for (n=17). The height was changed five times (450,337.5,225,168.75,112.5) µm when the diameter value (d = 450 µm), and as is evident in the chart, the value of Nu increases as the height of the jet decreases and the best Nu value was at the height value (L=112.5 µm). because as the height decreases, the effect of the cross-flow decreases, and the area in which the heat transfer occurs increases.

Fig. 7.b represents the relationship between height change and pressure drop at (d = 450 µm), (n=17), The height has been changed five times and fix the value of e at two values (1500,3000) note from the chart that the pressure drop increases as the height decreases and the highest value of the pressure drop were at the height value (L=112.5 µm) the reason for this is that the lower the height (L), the smaller the cross-sectional area for the outlet, when the cross-section area increases, the velocity decreases, and when the cross-section area decreases, the velocity increases (velocity of crossflow). As the high velocity at the exit increases the heat exchange and therefore increases Nu, but also increases the pressure drop.

Fig. 8 represents the change of the performance factor with the change in the height in the circular jet, whereas we have noticed that the Nusselt number increases as the height decrease, but the pressure drop increases as well. The diameter was fixed at (d = 450µm) and the number of jets at (n = 11), and we note from the chart that the performance factor was better at a higher height.

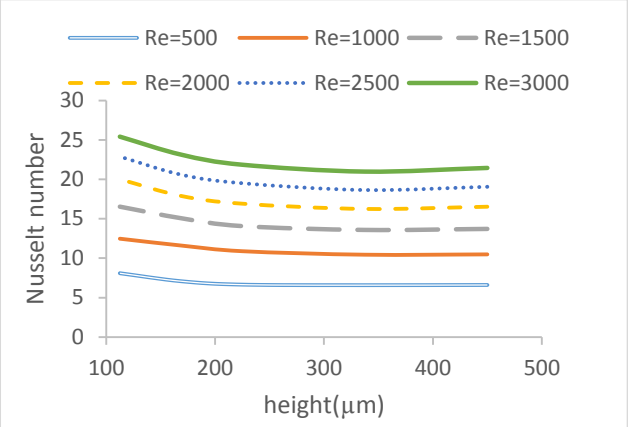

a

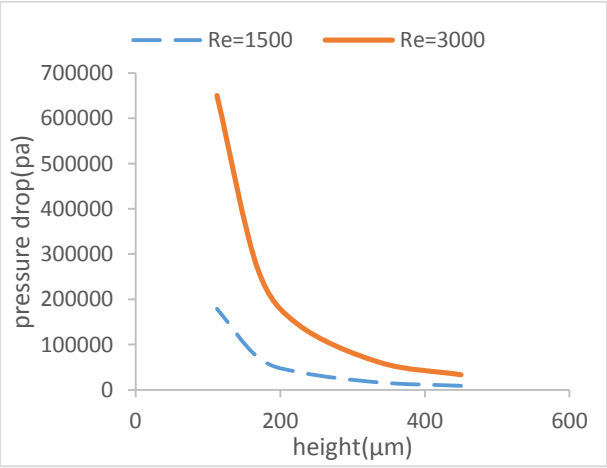

b

Fig. 7.a. Variation of Nusselt number (Nu) with height for (n=17) and (d=450 µm) in circular jet **b.** Variation of pressure drop (Δp) with height for two values of Re.

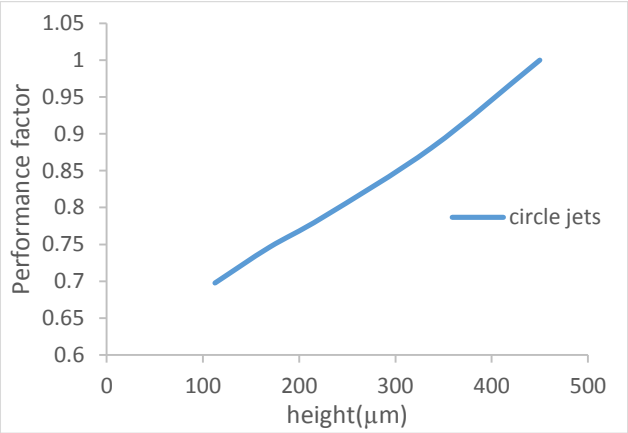

Fig.8 Variation of performance factor with height for the circular jet at (n=17) and (d=450µm)

4.4. effect of Jets number

Fig. 9 shows Variation of Nu with changing the number of jets in the circular jet, the number of Jets has changed five times (11,13,15,19,21), the value of height (L=450 µm), and for comparison, to find out which number gives a better value for the product, an average value of the diameter was chosen (d=450 µm) and drawn in the figure. As it is clear, when the number of jets increases, the value of Nu Increase this is because the flow rate increases when the number of the jet is increased and this increases the Nusselt number, and the best value when the number of jets does (n=21). Therefore (n = 21) was selected and a comparison of the diameters was made to find out which diameter we obtained the best value for Nu.

Fig. 10 represents variation of pressure drop with increasing number of jets at (d=450 µm), (L=450 µm), and the value of Re is fixed at two values (1500,2000), notice from the chart that the pressure drop increases with the increase in the number of jets, and its largest value is when the value of the number (n=21) the reason for this is that an increase in the number of jets leads to an increase in obstruction, as well as an increase in the cross flow that increases the pressure drop.

Fig. 11 represents variation of performance factor with the number of jets in the circular jet as the number (n= 21) has the highest value for of Nusselt number, but it also has the highest value for the pressure drop, so calculated the performance factor where the diameter value was fixed at (d = 150µm) and the height at (L = 450µm) and notice from the figure that the best value for the performance factor was at (n = 21) as it is the best in terms of increasing the cooling rate and less losses.

Fig. 12 (a-c) shows the velocity contours of the circular and square shapes where the velocity behavior is greatly influenced by cross-flow, which is the flow perpendicular to the inlet velocity, i.e. when it hit the wall opposite the jet, therefore, the velocity changes from the central jet to the last jet. The absence of crossflow at the first jet makes it hit the plate without deviating from the impinging area. The backflow continues to increase as we head towards the final jet which is subject to the greatest amount of backflow as the flow begins to deviate from the actual impinging area. This deviation is not apparent in the case of low speed, but it is more pronounced at the highest value of the speed, which increases the pressure drop as well.

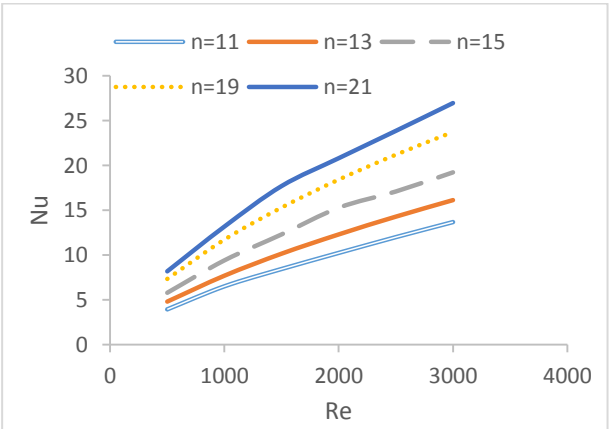

Fig. 9 Variation of Nusselt number (Nu) with Reynold number for five different jets number values in circular jets at (d=450 µm) and (L=450 µm)

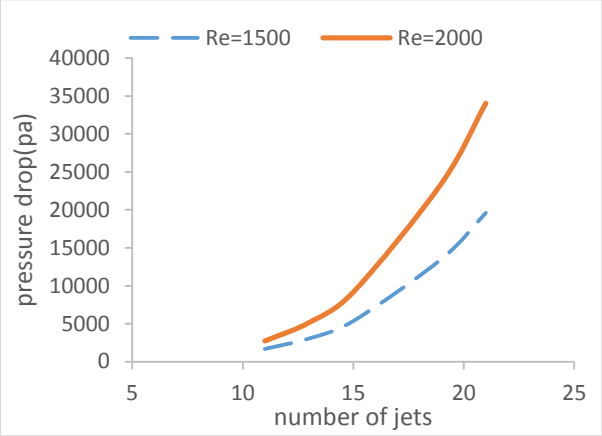

Fig. 10 Variation of pressure drop (Δp) with number of jets for two values of Re

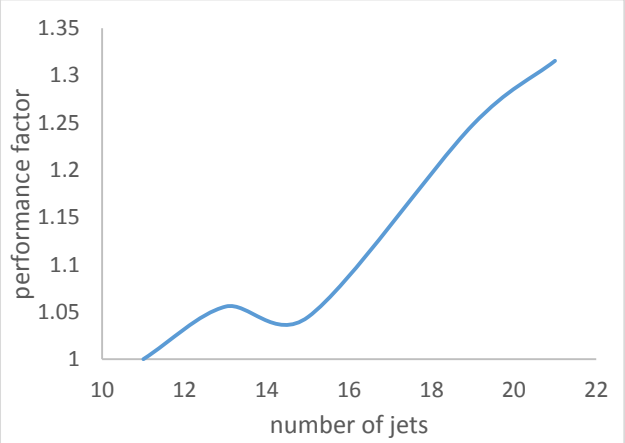

Fig. 11 Variation of jets number with performance factor for the circular jet at (L=450µm) and (d=150µm)

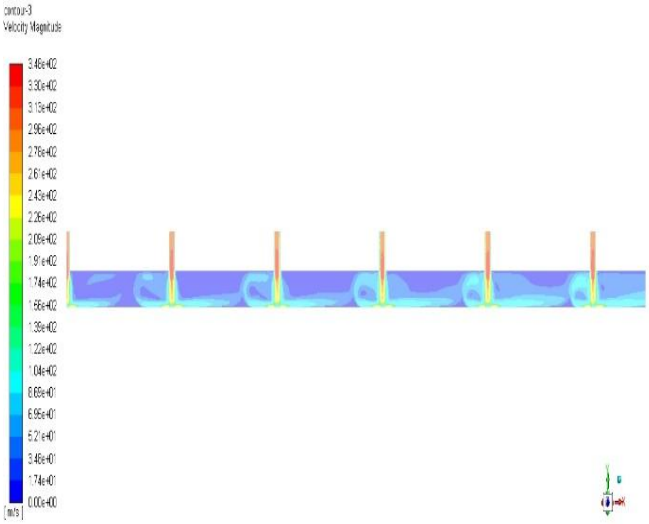

a-jets number =11, V=52.05m/s

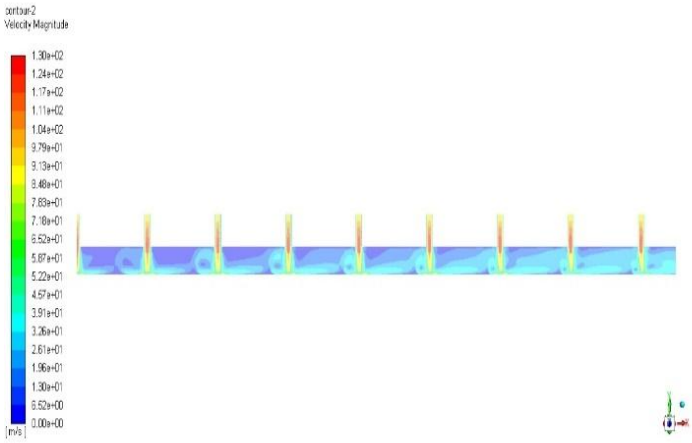

b-jets number=21, v=52.05m/s

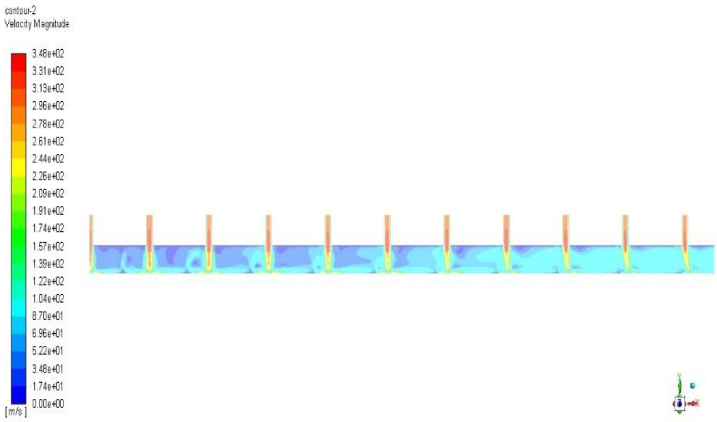

c-jets number=21, V=312.33 m/s

Fig. 12. Vertical contour of the velocity of circular jets at (d=150 µm) and (L=450µm) and in line arrangement

Conclusions:

The numerical simulation with impingement jet on the surface cooling has been done. This provides us with a basic concept of impingement cooling. And after discussing the results, the following conclusions were reached:

1.Increasing jets diameter does not only increase heat transfer coefficient (Nu), but rather reduces the pressure drop, thus increasing the performance of the micro jet, and the best value of (Nu) jet is when the diameter (d = 600 µm)

2.Reducing the distance between the jets and target increases the heat transfer coefficient, but it raises the pressure drop significantly. Therefore, the performance factor is better the higher the distance and the comparison between the circular and square shape in terms of the distance between jets and the target shows a match in pressure drop. This proves that the difference in pressure drop is due to the difference in the outlet area.

3.The heat transfer coefficient increases as the Reynolds number increases, as well as the pressure drop due to the increase in velocity.
4.The increase in the number of the jets leads to a significant increase in heat transfer coefficient and a decrease in the number of jets reduces the pressure drop, but the performance of micro jet when increasing the number of jets is better as the best value of performance parameter was at (n = 21).

References

[1] Hamdy Hassan, N.Y. Abdel Shafey," 3D study of convection-radiation heat transfer of electronic chip inside enclosure cooled by heat sink", International Journal of Thermal Sciences, 159 (2021) 106585.
[2] Wei T., Oprins H., Cherman V., Yang S., Wolf I.D., Beyne E., Baelmans M., "Experimental Characterization of a Chip Level 3D Printed Micro Jet Liquid Impingement Cooler for High-Performance Systems", IEEE Transactions on Components, Packaging and Manufacturing Technology, Vol. 9, NO. 9, (2019), PP. 1815-1824.
[3] Caliskan S., Baskaya S., Calisir T., ”Experimental and numerical investigation of geometry effects on multiple impinging air jets", International Journal of Heat and Mass Transfer, 75 (2014) 685‑703.
[4] Florschuetz L. W., Metzger D. E., and Truman C. R.," Jet array impingement with crossflow-correlation of stream wise resolved flow and heat transfer distributions", J. Heat Transfer, Vol. 103, No. 2, May 1981, PP. 337-342.
[5] Luo X. and Liu S." A Micro Jet Array Cooling System for Thermal Management of High-Brightness LEDs", IEEE Transactions on advanced packaging, VOL. 30, NO. 3, August (2007).
[6] Martin H." Heat and Mass Transfer Between Impinging Gas Jets and Solid Surfaces ","Adv. Heat transfer", Germany, 1977, Karlsruhe, PP.1-60.
[7] Xiao Bing L., Sheng L., XiaoPing J., Ting C." Experimental and numerical study on a micro jet cooling solution for high power LEDs", China Series E Technological Sciences, Vol. 50, No. 4, Aug. 2007.
[8] Browne E.A., Michna G.J., Jensen M.K., Peles Y." Experimental Investigation of Single-Phase Micro Jet Array Heat Transfer", Journal of Heat Transfer, (2010), Vol. 132.
[9] Husain A., Kim S.M., Kim K.Y.," Performance analysis and design optimization of micro-jet impingement heat sink", Heat Mass Transfer, Vol.10, (2013), PP. 1-12.
[10] Rattner A.S." General characterization of jet impingement array heat sinks with interspersed fluid extraction ports for uniform high-flux cooling", Journal of Heat Transfer, Vol. 139, August (2017), PP.1-11.
[11] Robinson A.J., Kempers R., Colenbrander J., Bushnell N., Chen R." A single phase hybrid micro heat sink using impinging micro-jet arrays and micro channel", Applied Thermal Engineering, Vol. 136, (2018), PP. 408-418.
[12] Zahoor R., Belšak G., Bajt S., Šarler1 B." Simulation of liquid micro-jet in free expanding high-speed co-flowing gas streams", Microfluidics and Nano fluidics, Vol. 10, (2018), PP. 22-87.
[13] Wei T., Oprins H., Cherman V., Beyne E., Baelmans M." Conjugate heat transfer and fluid flow modeling for liquid micro jet impingement cooling with alternating feeding and draining channels", Fluids, Vol. 4, (2019), PP. 145-164.
[14] Shin J., Rozenfeld T., Shockner T., Vutha A.K., Wang Y., Ziskind G., Peles Y.," Local heat transfer under an array of micro jet impingement using HFE-7000”, Applied Thermal Engineering, 158 (2019) 113716.
[15] Kumar K. V., and Jayahari L.," Study of Mechanical Properties and Wear Behavior of Aluminum 6063 Matrix Composites Reinforced with Steel Machining Chips", Materials Today: Proceedings, 5 (2018) 20285–20291.
[16] Penumadu P.S. and Rao A.G." Numerical investigations of heat transfer and pressure drop characteristics in multiple jet impingement system ", Applied Thermal Engineering, 110 (2017) 1511‑1524.
[17] Florian R. Menter," Zonal Two Equation k-w Turbulence Models for Aerodynamic Flows", 24th Fluid Dynamics Conference, July 6-9, 1993 / Orlando, Florida